

PCCP

Physical Chemistry Chemical Physics

Accepted Manuscript

This article can be cited before page numbers have been issued, to do this please use: C. D. Zeinalipour-Yazdi, *Phys. Chem. Chem. Phys.*, 2019, DOI: 10.1039/C9CP03934A.



This is an Accepted Manuscript, which has been through the Royal Society of Chemistry peer review process and has been accepted for publication.

Accepted Manuscripts are published online shortly after acceptance, before technical editing, formatting and proof reading. Using this free service, authors can make their results available to the community, in citable form, before we publish the edited article. We will replace this Accepted Manuscript with the edited and formatted Advance Article as soon as it is available.

You can find more information about Accepted Manuscripts in the [Information for Authors](#).

Please note that technical editing may introduce minor changes to the text and/or graphics, which may alter content. The journal's standard [Terms & Conditions](#) and the [Ethical guidelines](#) still apply. In no event shall the Royal Society of Chemistry be held responsible for any errors or omissions in this Accepted Manuscript or any consequences arising from the use of any information it contains.

Mechanisms of Ammonia and Hydrazine Synthesis on η - Mn_3N_2 -(100) Surfaces

View Article Online
DOI: 10.1039/C9CP03934A

Constantinos D. Zeinalipour-Yazdi^{a,b}

^a Department of Chemistry, University College London, 20 Gordon Street, London, WC1H 0AJ, UK

^b School of Science, University of Greenwich, Central Avenue, Chatham Maritime, Kent ME4 4TB, UK

*Corresponding author: c.zeinalipouryazdi@greenwich.ac.uk

Abstract

Understanding the mechanism of catalytic reactions is crucial for the future development of catalysts. In this computational study, dispersion-corrected Density Functional Theory (DFT) theory was used to calculate the various mechanistic pathways for ammonia and hydrazine synthesis on η - Mn_3N_2 -(100) surfaces. A simple Lewis structure representation algorithm was used in order to locate various possible N_xH_y intermediates. Hydrogenation of dinitrogen results in significant activation of the inert triple bond and these intermediates have a significant role in the ammonia and hydrazine synthesis reaction on manganese nitrides via a Langmuir-Hinshelwood mechanism. It is anticipated that these findings are significant in developing new catalysts for hydrazine synthesis using η - Mn_3N_2 (100) catalysts.

keywords: DFT, ammonia synthesis, manganese nitride, intermediates, IR

Introduction

Industrial ammonia synthesis via the Haber-Bosch (H-B) process¹⁻³ operates at a global annual production rate of ca. 174 million tonnes.⁴ It uses a $\text{Fe-K}_2\text{O-Al}_2\text{O}_3$ catalyst that operates under high temperatures (>400°C) and pressures (150-200 atm).

It is, therefore, an energy-intensive process and improvement of the catalysis would be socio-economically beneficial. Some newer industrial plants use the Kellogg advanced ammonia process that uses a graphite-supported alkali/alkaline-earth promoted Ru catalyst, which operates at milder conditions but is expensive.⁵ We are currently seeking catalytic materials and/or processes that could potentially produce ammonia at moderate temperatures ($T = 200\text{-}300\text{ }^{\circ}\text{C}$) in order to save energy.⁶ This would maximise production yield as it would shift the equilibrium of the nitrogen to ammonia synthesis reaction towards the products according to Le Chatelier's principle as ammonia synthesis is an exothermic reaction.

We have recently determined that ammonia synthesis can follow different reaction pathways on the very active cobalt molybdenum nitride ($\text{Co}_3\text{Mo}_3\text{N}$) catalyst⁷⁻¹² when nitrogen surface vacancies are present.¹³ Such vacancies are present in large concentrations even at ambient temperatures (i.e. 10^{13} cm^{-2}) and can efficiently activate N_2 .¹⁴ Other recent DFT studies determined that N-vacancies can participate in the mechanism for the electrochemical reduction of ammonia on Zr, Nb, Cr, V mononitrides¹⁵⁻¹⁶ and in the two-step solar-energy driven ammonia synthesis on metal-nitrides.¹⁷⁻¹⁸ It is, therefore, evident that the inclusion of nitrogen vacancies, either *intrinsic* or *extrinsic* in a mechanism of ammonia synthesis on metal nitrides may lead to the possibility of new lower energy mechanistic pathways.

There are three possible reaction mechanisms for ammonia synthesis on catalysts. The most accepted mechanism is the Langmuir-Hinshelwood (L-H) mechanism, which is the mechanism that takes place on the iron¹⁹⁻²⁰ and ruthenium^{12, 21-22} catalyst. In addition to this general mechanism which is dissociative, other associative mechanism²³ which follow Mars-van Krevelen (MvK) and Eley-Rideal (E-R) mechanisms have been recognised for ammonia synthesis on metal nitrides.^{13-14, 24}

In this study we have investigated such mechanisms for ammonia and hydrazine synthesis on the (100) surface of $\eta\text{-Mn}_3\text{N}_2$. We have also used accurate IR simulations using hybrid DFT to identify various intermediates for the ammonia and hydrazine synthesis reactions which is crucial for the validation of reaction mechanism from *in situ* and *operando* surface analytical techniques.

Initially we used Lewis representations to predict various possible surface intermediates for the ammonia and hydrazine synthesis reactions. These intermediates were fully optimised using the B3LYP XC functional and relatively large basis sets, in order to sample a broad configurational space and to see which Lewis structures would yield stable geometries for the intermediates. Out of the 18 Lewis structures with stoichiometries N_xH_y (where $x \leq 2$ and $y \leq 3$) we found that there are eight stable intermediates for the ammonia and hydrazine synthesis reaction. These intermediates were then used to build various potential mechanisms for hydrazine and ammonia synthesis on the surface of η - Mn_3N_2 . For these adsorbates we have calculated the atomic charges and the infrared spectrum to assist experimental efforts for their identification. Our detailed computational study determined that side on activated surface di-nitrogen becomes further activated due to hydrogenation reactions that result in the formation of $HN=NH$ and hydrazine which is bound to the surface of the catalyst at four-fold nitrogen vacancies.

1. Computational Methods

1.1 Surface Calculations

In order to model the bulk and surfaces of η - Mn_3N_2 we have used the coordinates as determined by powder neutron diffraction (ND) at ambient temperature.²⁵ This material was chosen for the catalytic studies among other manganese nitrides as there is experimental evidence that it easily loses the lattice nitrogen, which would generate a large number of nitrogen vacancies.²⁶ The bulk unit cell of η - Mn_3N_2 is an fcc arrangement of Mn with N occupying the octahedral sites. This unit cell is face-centred tetragonal with the following lattice parameters, $a = 4.2046 \text{ \AA}$, $b = 4.2046 \text{ \AA}$, $c = 12.1311 \text{ \AA}$, $\alpha = \beta = \gamma = 90^\circ$.²⁵ The (100) surface was modelled via a slab of a thickness of 6.3 \AA measured between the centers of two surface Mn atoms (the surface unit cell is given in Fig. 3). The slab model had a 20 \AA vacuum gap from which the various adsorbates were let to interact with the surface. All DFT calculations were periodic Γ -point centered with a $3 \times 5 \times 1$ Monkhorst-Pack grid²⁷ spin-polarised obtained with the use of the VASP 5.4.1 code.²⁸⁻²⁹ Exchange and correlation effects were considered within the generalized gradient approximation (GGA) using the revised Perdew-Burke-Ernzerhof (revPBE) exchange-correlation (XC) functional,³⁰ with the projector augmented-wave (PAW) method³¹⁻³² used to

represent core states. These were 1s to 3p for Mn and 1s for N and H. The cut-off energy for the energy of the planewaves was 600 eV. Geometry optimizations were performed with a residual force threshold on each atom of 0.01 eV Å⁻¹ using the conjugate-gradient algorithm. The electronic relaxation convergence criterion was set to 10⁻⁴ eV. The initial charge density was obtained by superposition of atomic charges. Initial adsorption configurations were such that the distance between the adsorbate and the nearest surface site was roughly that of the adsorbate-cluster distance. The various adsorption sites were every symmetry unique surface site determined in Figure 3, which resulted in 5 sites for the (100) surface. The adsorption energy was taken as the total energy difference between the fully relaxed bound state of the surface-adsorbate complex from that of the fully relaxed surface slab and the isolated molecules given by:

$$\Delta E_{\text{ads, D3}} = E_{\text{slab-adsorbate}} - E_{\text{slab}} - E_{\text{adsorbate}} \quad (1).$$

Dispersion corrections were included via the zero-damping DFT-D3 correction method of Grimme as implemented in VASP,³³ in which the following dispersion energy correction is added to the Kohn-Sham energies,

$$E_{\text{disp}} = -\frac{1}{2} \sum_{i=1}^N \sum_{j=1}^N \left(s_6 \frac{C_{6,ij}}{r_{ij}^6} + s_8 \frac{C_{8,ij}}{r_{ij}^8} \right), \quad (2)$$

where $C_{6,ij}$ and $C_{8,ij}$ denote the averaged (isotropic) 6th and 8th order dispersion coefficients for atom pair ij and r_{ij} is the internuclear distance between atoms i and j , respectively, s_6 and s_8 are the functional-dependent scaling factors.

To model the Potential Energy Surface (PES) of the various reaction mechanisms we have used activation barriers that were calculated with the nudged elastic band (NEB) method as implemented in VASP³⁴, using 5 images. The relative energies calculated in the PES are total electronic energy differences with respect to the reference state $A + N_2(g) + 3H_2(g)$. In our computational analysis of the reaction mechanism the surface stoichiometry of the bulk crystal of Mn₃N₂ is maintained as we have only considered reactions in which the lattice nitrogen removed originates from the nitrogen adsorbed from the gas phase. This excludes the possibility of lattice degradation, which under certain conditions (e.g. T, P, feedstream composition) could cause phase transitions of Mn₃N₂ to other phases.³⁵⁻³⁶

1.2 Cluster Calculations

Hybrid DFT computations have been performed with Gaussian 09³⁷ with the use of Becke's three-parameter hybrid exchange functional³⁸ (XC) combined with the Lee-Yang-Parr non-local correlation functional³⁹, abbreviated as B3LYP. For the basis functions, we have used the spherical version (5d, 7f), the correlation consistent augmented valence triple zeta basis set⁴⁰⁻⁴⁴, abbreviated as aug-cc-pVTZ for N and H and an ECP-121G⁴⁵⁻⁴⁷ basis set for Mn. Dispersion forces were accounted for with the D3 method by Grimme as implemented in Gaussian 09.³³ This computational methodology is abbreviated as B3LYP-D3/ECP-121G(Mn),aug-cc-pVTZ(N,H). The cluster on which the binding studies were done, was a tetrahedral Mn₃N cluster depicted in Figure 2 (A). This cluster belonged to the C_{3v} point group with a Mn-Mn bond of 2.113 Å and a Mn-N bond of 1.816 Å. The cluster adsorbate models were fully optimised and the stationary points have been confirmed using vibrational analysis, by the absence of imaginary vibrational frequencies. The SCF convergence criteria for the root mean square (RMS) density matrix and the total energy were set to 10⁻⁸ Hartrees/Bohr and 10⁻⁶ Hartrees, respectively.

2 Results and Discussion

2.1 Locating potential adsorbates via Lewis representations

In order to elucidate computationally a reaction mechanism it is critical to understand the structure of various active intermediates that participate in the reaction mechanism and are not spectator species. Here we have used Lewis representations to find possible structures of the intermediates of the ammonia and hydrazine synthesis reaction. An adsorbate that participates in the surface chemical reaction was constructed having a particular stoichiometry (e.g. NH, N=NH, HN=NH) by Lewis representations and then tested how well it interacts with the surface of a cluster model and the surface of the metal nitride. The structures that were generated using Lewis representations are depicted in Figure 1 and are based on the following algorithm: (i) assume that these adsorbates are not charged, (ii) nitrogen follows the octet-rule (i.e. the rule of eight⁴⁸) (iii) nitrogen is bound to the manganese atoms of the substrate and not nitrogen of the metal nitride cluster (i.e. this excludes the formation of azido compounds that we observed to form on tantalum nitrides⁴⁹) and (iv) that each substrate-N bond is due to equal sharing of one electron from nitrogen

and one electron from the manganese atom. Additionally, for the 3D design of the adsorbates we have taken into account four design criteria for the nitrogen atoms (i) that when they bond to four chemical groups (e.g. 4 single bonds) they are tetrahedrally coordinated, (ii) that when they are bond to three electron groups (e.g. a double bond, a single bond and a lone electron pair) they are trigonally coordinated, (iii) that when they bond to two electron groups (e.g. a single bond and a triple bond) then they have linear configurations and (iv) that the dinitrogen configuration can be either *end-on*, *side-on* or *tilt end-on* based on the binding dinitrogen on another metal nitride.¹⁴ This approach significantly reduced the configurational space of the 3D structures that could be constructed using Lewis representations. From this algorithm generated 18 possible structures depicted in Figure 1 for N_xH_y adsorbates, where $x \leq 2$ and $y \leq 3$, that were designed to be bound to a Mn_3N cluster and optimised using various starting structures. The resulting converged structures for these adsorbates are depicted in Figure 2. These structures are also given as supporting information in Figure S1. We found that cluster adsorbate calculations did serve as a computationally inexpensive model which could identify stable structures of the various intermediates using hybrid-DFT and a relatively large basis set with additional diffuse and polarisation functions. The intermediates identified from the cluster approach were then used to model the various intermediates on the surface of η - Mn_3N_2 (100) surfaces. In some cluster-adsorbates, we had to add a charge in order to find a stable structure for the adsorbate (i.e. **D**, **F**, **H** and **I**). However, these calculations are computationally inexpensive and need only a few hours to converge on a dual-core machine. Therefore, we could screen a large number of different starting geometries to sample thoroughly the configurational space of N_xH_y adsorbates, where $x \leq 2$ and $y \leq 3$. Additionally we were able to obtain accurate IR oscillator frequencies of the various intermediates which are given in section 2.4.

View Article Online
DOI: 10.1039/C9CP03934A

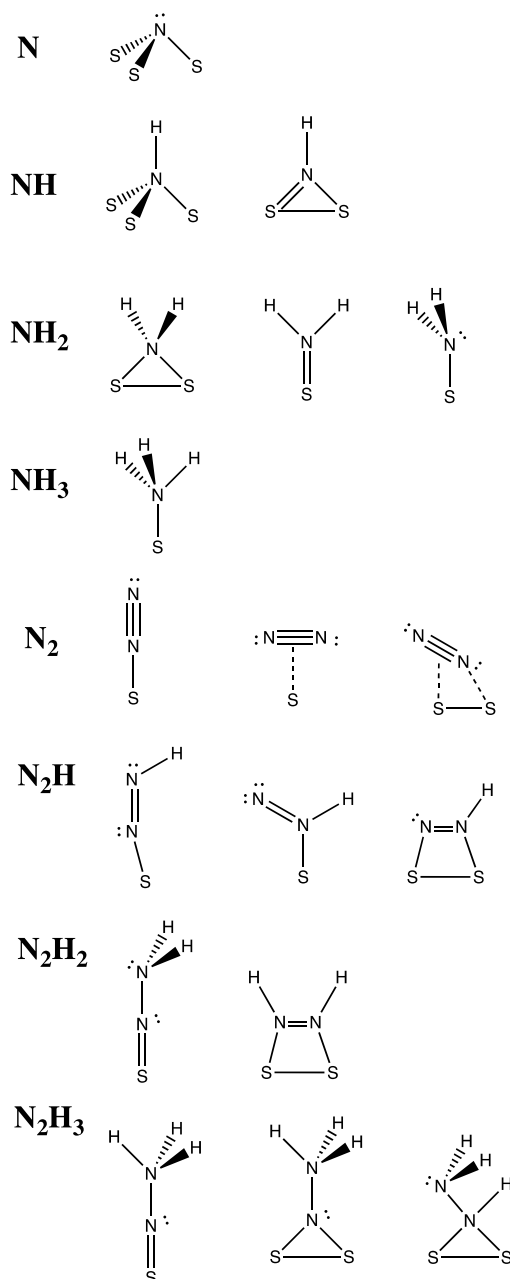


Figure 1. Lewis structures of various possible intermediates N_xH_y ($x = 1, 2$ and $y = 1, 2, 3$) on a three-fold hollow of the substrate. The symbol 'S' refers to a substrate atom which for the model system under investigation is a 'Mn' atom.

2.2 APT charge analysis

There are various methods to derive atomic charges. We have used the atomic polar tensor (APT) method to obtain atomic charges. This charge population analysis has the advantage of being invariant with respect to changes to the coordinate system.⁵⁰

The charge analysis determines that in all structures the nitride nitrogen has a negative charge of about $-0.5 |e|$, which is counterbalanced by a positive charge of the Mn_3 cluster. All hydrogens have a positive charge of $0.1 |e|$ to $0.3 |e|$. The negative charge on the nitrogen atoms can be used as a descriptor for protonation reactions as we describe next. Adsorbate **C** and **D** have a negative charge of $-0.539 |e|$ and $-0.479 |e|$, respectively, which indicates that they will be very reactive with H^+ or atomic hydrogen that is bound to the metal nitride. Interestingly, the charges on adsorbate **E**, dinitrogen are positive $0.5 |e|$ on the nitrogen directly bound to the cluster, whereas negative $-0.5 |e|$, on the second nitrogen, which indicates that the second nitrogen is more reactive for nucleophilic substitution reactions. This factor could be relevant to the formation of the hydrazinylidene intermediate, $=NNH_2$, found in our earlier study of the mechanism of ammonia synthesis on cobalt molybdenum nitride.¹³ Among the other four diazene and diazane adsorbates found, **F** based on the negative charge of the terminal nitrogen will be very reactive towards hydrogen, which will form $-NNH_2$. It is notable that we were not able to find a stable structure for $-NH_3$ bound to the cluster, however, ammonia was found to form a stable bond with Mn atoms at nitrogen vacancies of the surface model, as determined in a subsequent section. In the following section we study in the presence and absence of dispersion interactions the binding energy of the adsorbate to the Mn_3N cluster.

View Article Online
DOI: 10.1039/C9CP03934A

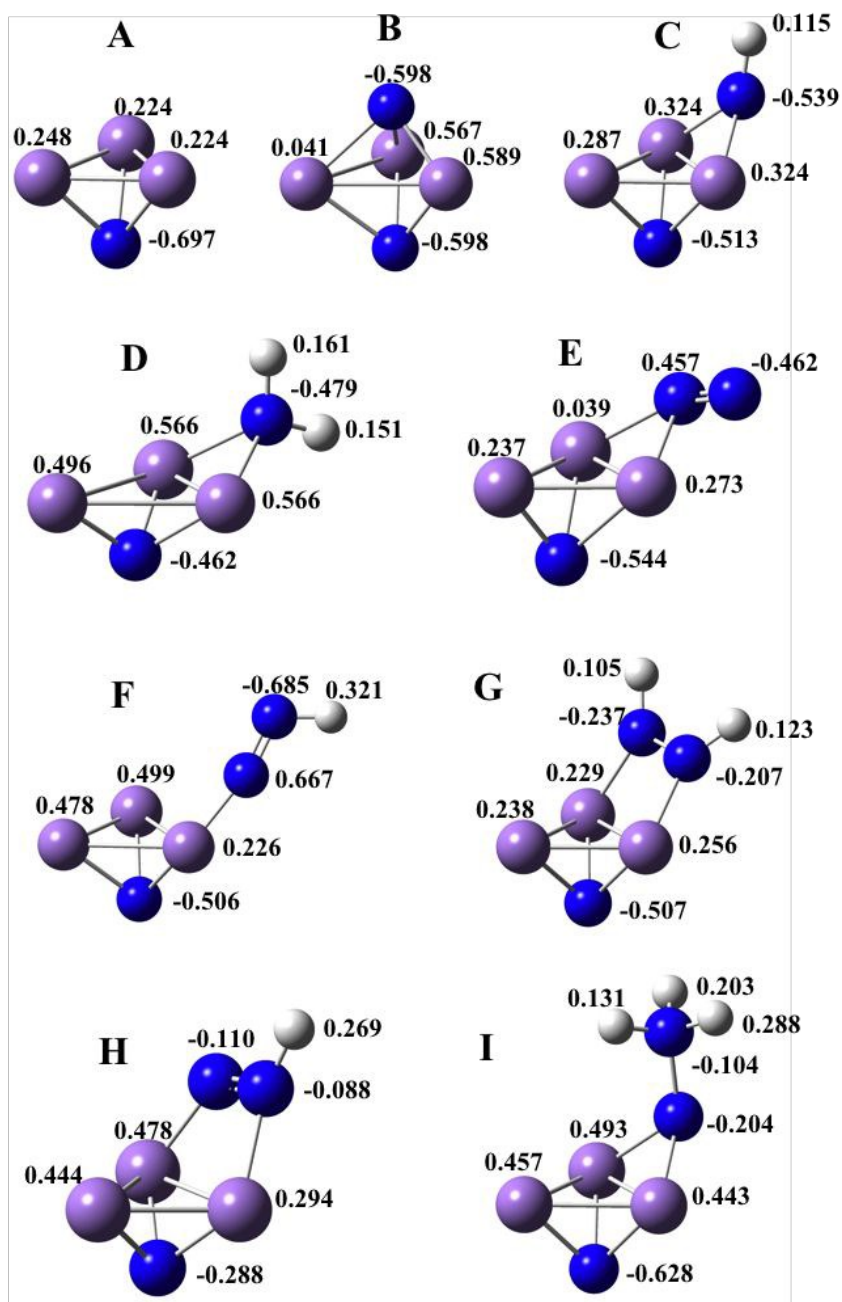


Figure 2. Atomic polar tensor (APT) population analysis for the various ammonia synthesis adsorbates (N, NH, NH_2 , $N=NH$, $HN=NH$, NNH_3 and N_2) on a Mn_3N cluster.

2.3 Structures and binding energies of adsorbates to Mn_3N

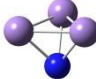
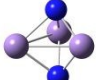
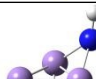
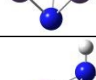
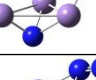
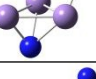
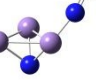
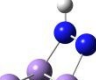
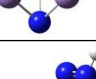
In table 1 we depict the various adsorbates that we determined based on Lewis structures bound to the Mn_3N cluster. **A** and **B** are nitrides, **C** is an azanediyl adsorbate, **D** an azanylium adsorbate and **E** dinitrogen, all of which are known adsorbates of inorganic nitrogen-containing compounds. Furthermore, **G** resembles

hydrazine-1,2-diyl and **I** diazan-2-ium-1-ide, of which the last was identified as an important intermediate in the mechanism of ammonia synthesis via an Eley-Rideal / Mars van Krevelen mechanism.¹³ For **F** we could not find the corresponding inorganic adsorbate and it may, therefore, be an unstable intermediate or an adsorbate that is currently not identified. Furthermore, the doubly substituted diazane adsorbate, **G** has not been previously considered in the mechanism for ammonia synthesis and therefore we further tested its adsorption on η -Mn₃N₂ surfaces that contain intrinsic nitrogen vacancies. We also test the binding of **H** to η -Mn₃N₂ surface as this may represent the state of the adsorbate after its first hydrogenation reaction on the surface of the catalyst.

The binding energy of these adsorbates was evaluated in Table 1 with (ΔH_{bind}) and without ($\Delta H_{\text{bind,D3}}$) the semi-empirical correction for the dispersion interaction as given by Grimme's D3 scheme. In some cases (i.e. **I**) the binding energies mostly due to the polarizable nature of the N \equiv N bonds differs by 21 kJ mol⁻¹ from the uncorrected values, indicating that the D3-correction is necessary to obtain accurate thermochemical adsorption data for nitrogen-containing compounds on Mn. The only adsorbate that is weakly bound is dinitrogen with a binding energy of 79 kJ mol⁻¹, consistent with the weak, adsorption we have previously found on other metal nitrides.^{14, 49} It is intriguing to observe that the binding energy of all other adsorbates is very strong which can at least in part be explained by the bonding to a small cluster rather than a surface and maybe a result of the better overlap between filled orbitals of the adsorbate and the empty d-orbitals of Mn on Mn₃N. The dispersion correction for all adsorbates makes the binding energy more exothermic by an average value of -12 kJ mol⁻¹, which is only a small portion of the total binding energy. This indicates that the bonds formed between adsorbate and cluster are primarily ionic and covalent and only a small portion of the binding energy can be attributed to dispersion forces. In cases where the adsorbate adsorption energy is weak the overall contribution of the dispersion forces is greater and this is observed for the adsorption of dinitrogen. We have therefore made all surface-adsorbate calculations invoking the D3 correction.

In the next section, we study the IR wavelength and absorption intensities of the various adsorbates bound to the Mn₃N cluster.

Table 1. Tabulated structures, labels, spin multiplicity (s.m.), charge and binding enthalpies with ($\Delta H_{\text{bind,D3}}$) and without D3 correction (ΔH_{bind}) of various N_xH_y ($x = 1, 2$ and $y = 1, 2, 3$) obtained at B3LYP-D3/ECP-121G(Mn), aug-cc-pVTZ(N,H) level of theory.

Label	Structure	s.m.	charge	ΔH_{bind} (kJ mol ⁻¹)	$\Delta H_{\text{bind,D3}}$ (kJ mol ⁻¹)
A		1	0	–	–
B		2	0	-1421	-1423
C		1	0	-713	-722
D		1	+1	-1041	-1055
E		1	0	-79	-85
F		1	+1	-440	-451
G		1	0	-285	-302
H		1	+1	-523	-535
I		1	+1	-816	-837

2.4 Infrared oscillator frequencies of various adsorbates

For every cluster-adsorbate determined in Table 1 we have obtained converged calculations of the analytical Hessian, which yielded the oscillator frequencies and intensities. These are listed in Table 2 and can be used as a guide for the experimental determination of some of these adsorbates in inorganic compounds. They could also be used as a guide to spectroscopically determine new ammonia and hydrazine synthesis reaction intermediates on solid manganese nitride catalysts.

For **A** the infrared spectrum is simple with two low frequency vibrational bands at 370 cm^{-1} and 827 cm^{-1} corresponding to the vibrational stretching frequency of the Mn-Mn and Mn-N bond, respectively, which indicates the Mn-N bond is generally stronger than the Mn-Mn bond in these metal nitrides, which explains why the formation of metal nitrides increases the hardness of these materials. The IR spectrum of **B** is very similar to **A** as the type of chemical bonding remains the same in the structures. Therefore, the nitride adsorbate could be identified by the stretching frequency of the Mn-N bond, which is between 800 cm^{-1} to 850 cm^{-1} . The azanediyl (i.e. **C**) adsorbate can be identified by an additional weak band at 3451 cm^{-1} which corresponds to the vibrational stretching frequency of the $>\text{N-H}$ bond. The azanylium (i.e. **D**) adsorbate could be identified (Id. in table 2) by the two symmetric (3411 cm^{-1}) and anti-symmetric (3494 cm^{-1}) stretching frequencies of the $-\text{NH}_2^+$ group. Adsorbate **E** (i.e. dinitrogen) can be identified by the very strong in intensity IR band ($662 \times 10^{-40}\text{ esu}^2\text{ cm}^2$) at 1781 cm^{-1} . Adsorbate **F** has a similar band for the $\text{N}=\text{N}$ band as dinitrogen found at 1779 cm^{-1} . However, in addition, it can be identified by a stretching band of the N-H group found at 3267 cm^{-1} , consistent with the experimental vibrational band of N-H in amides which ranges between 3100 cm^{-1} to 3500 cm^{-1} .⁵¹

The various N_xH_y adsorbates can be identified by their very different positions of the $\text{N}=\text{N}$ stretching band. This band has a moderate intensity that ranges between 65.2 to $644.7 \times 10^{-40}\text{ esu}^2\text{ cm}^2$ and should, therefore, be clearly visible in the actual IR spectrum. We also find that the degree of hydrogenation determines the bond order (B.O.) of the N-N bond, which has a B.O. of 1 to 3. The smaller the bond-order, the weaker the oscillator frequency that is observed in the IR spectrum. In particular, adsorbate **I** has a vibrational frequency of only 550 cm^{-1} due to its single bond and only one adjacent lone electron pair, based on its Lewis structure. Adsorbate **G** has again a single bond N-N and two lone electron pairs on the nitrogen which increase somewhat the B.O. of the N-N and, therefore, its vibrational frequency becomes 951 cm^{-1} . Adsorbate **H** has a double bond between $\text{N}=\text{N}$, and therefore, its vibrational frequency becomes 1325 cm^{-1} . It is therefore, possible to identify the degree of hydrogenation of these intermediates by the relative shift of this IR band to lower frequencies. To summarise these results it is notable that the bonds between the two nitrogen in di-nitrogen, diazanes and diazenes decreases in strength as a function of hydrogen substitution and adsorbate coordination as determined in scheme 1, which

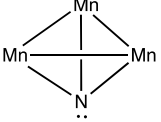
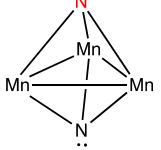
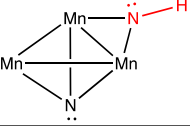
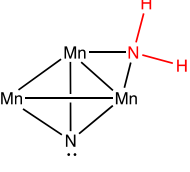
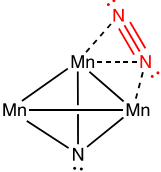
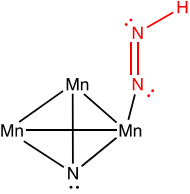
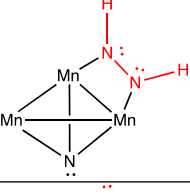
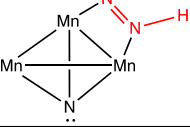
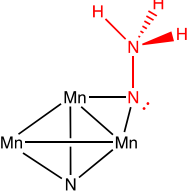
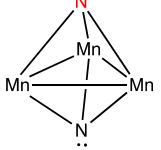
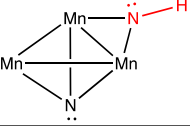
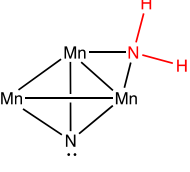
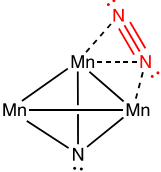
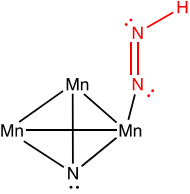
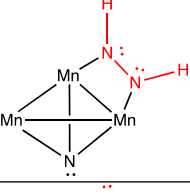
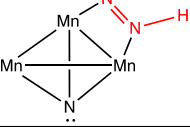
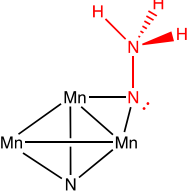
can be clearly seen in adsorbates **E**, **F**, **H**, **G** and **I** which have a successively lower frequency vibrational band for the N-N bond, with frequencies of 1781 cm⁻¹, 1779 cm⁻¹, 1325 cm⁻¹, 951 cm⁻¹ and 550 cm⁻¹, respectively. Therefore, the stretching frequency of the N-N bond should be used by experimentalist to assess the degree of hydrogenation of nitrogen-containing compounds on the surface of metal-nitride catalysts.

We, therefore, recommend that these computational results can assist experimental efforts to identify new intermediates for the ammonia and hydrazine synthesis reaction using techniques such as attenuated total reflectance (ATR) and diffuse reflectance (DRIFTS) infrared spectroscopy.

In the next section, we study the various adsorption sites of diazene and diazane intermediates, such as the one found in structures **G** and **H** on the (100) surface of η -Mn₃N₂.

Table 2. Infrared vibrational frequencies (ν_{IR}), mode and intensities (I_{IR}) of various N_xH_y ($x = 1, 2$ and $y = 1, 2, 3$) adsorbates on Mn_3N cluster obtained at B3LYP-D3/ECP-121G(Mn), aug-cc-pVTZ(N,H) level of theory.

View Article Online
DOI: 10.1039/C9CP03934A

Label	Structure	ν_{IR} (cm^{-1})	I_{IR} (10^{-40} esu 2 cm 2)	mode	Id. (cm^{-1})																																																																																																								
A		827	139.9	Mn-N stretching Mn-Mn stretching	827																																																																																																								
		370	7.1			B		836	32.4	Mn-N sym stretching Mn-N anti-sym-stretch. Mn-N bending stretch. Mn-Mn stretching	836	693	108.9	457	91.1	<247	3.6	C		3451	2.5	N-H stretching N-H bending Mn-N stretching Mn-Mn stretching	3451 797	797	37.3	776/789	119.5/48.2	<443	1.0	D		3494	41.2	H-N-H anti-sym stretching H-N-H sym stretching H-N-H bending (scissor) H-N-H bending (rocking) Mn-N stretching Mn-NH $_2$ stretching	3494 3411	3411	31.4	1576	20.8	817	89.9	653	13.1	625	37.4	E		1781	662.3	N=N stretching Mn-N stretching Mn-N $_2$ stretching Mn-Mn stretching	1781	821	112.2	564	23.4	<382	3.8	F		3267	94.7	N-H stretching N=N stretching N-H bending Mn-N stretching	3267 1779	1779	644.7	1129	373.8	<785	64.5	G		3438	4.9	N-H sym stretching N-H anti-sym stretching N-H anti-sym bending N-H sym bending N=N stretching Mn-N stretching	951	3428	0.9	1397	29.3	1234	8.7	951	114.8	H		734	59.3	N-H stretching N=N stretching N-H bending Mn-N bending	1325	3371	90.4	1325	181.8	1308	108.8	I		776	19.9	N-H anti-sym stretching N-H sym stretching N-H anti-sym bending (scissor) N-H sym bending (scissor) Mn-N stretching N-N stretching	550	3468	64.1	3345	2.8	1645	50.5	1432	104.5
B		836	32.4	Mn-N sym stretching Mn-N anti-sym-stretch. Mn-N bending stretch. Mn-Mn stretching	836																																																																																																								
		693	108.9																																																																																																										
		457	91.1																																																																																																										
		<247	3.6																																																																																																										
C		3451	2.5	N-H stretching N-H bending Mn-N stretching Mn-Mn stretching	3451 797																																																																																																								
		797	37.3																																																																																																										
		776/789	119.5/48.2																																																																																																										
		<443	1.0																																																																																																										
D		3494	41.2	H-N-H anti-sym stretching H-N-H sym stretching H-N-H bending (scissor) H-N-H bending (rocking) Mn-N stretching Mn-NH $_2$ stretching	3494 3411																																																																																																								
		3411	31.4																																																																																																										
		1576	20.8																																																																																																										
		817	89.9																																																																																																										
		653	13.1																																																																																																										
		625	37.4																																																																																																										
E		1781	662.3	N=N stretching Mn-N stretching Mn-N $_2$ stretching Mn-Mn stretching	1781																																																																																																								
		821	112.2																																																																																																										
		564	23.4																																																																																																										
		<382	3.8																																																																																																										
F		3267	94.7	N-H stretching N=N stretching N-H bending Mn-N stretching	3267 1779																																																																																																								
		1779	644.7																																																																																																										
		1129	373.8																																																																																																										
		<785	64.5																																																																																																										
G		3438	4.9	N-H sym stretching N-H anti-sym stretching N-H anti-sym bending N-H sym bending N=N stretching Mn-N stretching	951																																																																																																								
		3428	0.9																																																																																																										
		1397	29.3																																																																																																										
		1234	8.7																																																																																																										
		951	114.8																																																																																																										
H		734	59.3	N-H stretching N=N stretching N-H bending Mn-N bending	1325																																																																																																								
		3371	90.4																																																																																																										
		1325	181.8																																																																																																										
		1308	108.8																																																																																																										
I		776	19.9	N-H anti-sym stretching N-H sym stretching N-H anti-sym bending (scissor) N-H sym bending (scissor) Mn-N stretching N-N stretching	550																																																																																																								
		3468	64.1																																																																																																										
		3345	2.8																																																																																																										
		1645	50.5																																																																																																										
		1432	104.5																																																																																																										
		804	102.4																																																																																																										
550	65.2																																																																																																												

2.5 Adsorption of HN=NH and N=NH on η -Mn₃N₂ surface

View Article Online
DOI: 10.1039/C9CP03934A

Table 3. Adsorption energy, percent activation and selected structural parameters for optimised structures of HN=NH and N=NH on η -Mn₃N₂-(100) surface calculated with $E_{\text{cut}} = 600$ eV, a 3x5x1 gamma-point MP grid and the revPBE functional. Fractional coordinates of the various structures are given as supporting information Figure S2.

Property	site 1	site 2	site 3	site 4	site 5	site 1	site 2	site 3	site 4	site 5	Units
	HN=NH					N=NH					
$\Delta E_{\text{ads,D3}}$	-155	-133	-134	-103	-184	-150	-135	-138	-178	-181	kJ/mol
$r(\text{N-N})$	1.336	1.323	1.323	1.394	1.424	1.283	1.277	1.279	1.375	1.374	Å
$a(\text{Mn-N-N})^{\text{a}}$	114.6	108.3	108.3	130.7	113.8	114.7	109.1	109.1	114.5	114.6	°
$r(\text{N-H})^{\text{b}}$	1.027	1.028	1.026	1.031	1.028	1.030	1.033	1.032	1.030	1.033	Å
$r(\text{Mn-N})^{\text{c}}$	1.974	2.006	2.006	2.142	2.074	1.896	1.941	1.934	2.009	2.032	Å
N_2 activation ^c	18	17	17	22	24	14	13	14	21	21	%

^a Angle taken as average of two angles

^b Bond length taken as average of two bonds when two N-H groups present

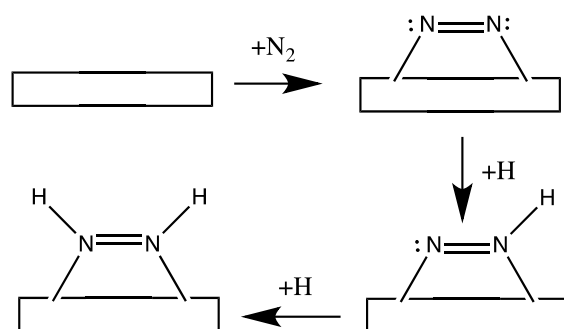
^c Bond length taken as average of two bonds

^d Percent activation is defined as $[\text{r}(\text{N}_2\text{H}_2, \text{ads}) - \text{r}(\text{N}_2, \text{g})] * 200 / [\text{r}(\text{N}_2, \text{g}) + \text{r}(\text{N}_2\text{H}_2, \text{ads})]$

The adsorption of N₂, HN=NH and N=NH was studied on the surface of η -Mn₃N₂ using periodic DFT-D3 calculations. The results for HN=NH and N=NH are presented in Table 3. We have calculated the adsorption properties at five symmetry unique sites of the (100) surface of η -Mn₃N₂, which are depicted in Figure 3. The adsorption of N₂ was found to be molecular at these five sites and very weak (-12 kJ mol⁻¹ to 38 kJ mol⁻¹). In particular, only at the nitrogen-vacancy (**site 5**) was it adsorbed close to the surface in a side-on configuration, residing in the four-fold hollow and simultaneously bound to four Mn atoms ($\Delta E_{\text{ads,D3}} = 38$ kJ mol⁻¹). We anticipate that the N₂ adsorbed at **site 5** can undergo further hydrogenation reactions as presented in Scheme 1 in order to form the new intermediates of the ammonia synthesis reaction, N=NH and HN=NH. Dinitrogen activation at this site was calculated to be 12% which is comparable to the 11% activation of N₂ on Co₃Mo₃N-(111) surface, where, however, it was adsorbed in an end-on configuration.¹⁴ These calculated intermediates are therefore subsequently used in section 2.6 to model various reaction pathways for ammonia and hydrazine synthesis on the (100) surface of η -Mn₃N₂. Particular attention was given to mechanisms in which the intrinsic

nitrogen vacancies of this material actively participated in surface reactions, similar to the mechanisms of ammonia synthesis on cobalt molybdenum nitride.¹³

We next present the results for the adsorption of HN=NH and N=NH which are schematically depicted in Scheme 1 on the (100) surface of η -Mn₃N₂ at the five symmetry unique sites. Scheme 1 also depicts the hypothetical hydrogenation mechanism via L-H which for the ammonia synthesis reaction mechanism.



Scheme 1. Simplified schematic presenting the adsorption of N₂ to nitrogen vacancies on the surface of η -Mn₃N₂ and their successive hydrogenation.

For the adsorption of N=NH, the average bond length of the Mn-NH was found to be consistently 8% longer than the Mn-N bond length, which is consistent with the fact that the additional hydrogen reduces the partial negative charge on the nitrogen making the Mn-N weaker. The percentage activation of the N-N bond was found to be consistently larger (17 to 24 %) for HN=NH than for N=NH which was (13 to 21%), which indicates that hydrogenation reactions such as the one presented in Scheme 1 can cause further activation of the N-N bond, decreasing therefore the barrier for its dissociation (note that the bond dissociation enthalpy of N₂ is very high, 945 kJ mol⁻¹)⁵². The adsorption energies though of HN=NH and N=NH were found to be very similar. For all adsorption sites apart **site 4** the adsorption energy only differed by less than 5 kJ mol⁻¹ for HN=NH and N=NH. However, for **site 4** the adsorption configuration was found not to be the same for HN=NH and N=NH. In fact although both HN=NH and N=NH had the same starting structure which is presented in Figure 3 (**site 4**) for NH=NH, the optimised structure for N=NH was such that it resided side-on in the four-fold hollow simultaneously bound to four Mn atoms (these are the 4 surface Mn atoms surrounding the N-vacancy), which is consistent with Scheme 1 for the adsorption configuration of N₂. We, therefore,

observe that for all adsorbates studied (i.e. N_2 , $N=NH$ and $HN=NH$) it is only site 4 that results in an adsorbed configuration where the N-N bond is significantly activated. Furthermore, in this adsorbed configuration the nitrogen is adsorbed close enough to the surface Mn atoms so that hydrogenation reactions can occur. These hydrogenation reactions should weaken the N-N bond as they withdraw electronic charge from the occupied p and d electrons of Mn, which would become a facile route for activating the relatively inert triple bond of di-nitrogen.

To summarise, N_2 , $N=NH$ and $HN=NH$ can bind at nitrogen vacancy sites on the (100) surface of η - Mn_3N_2 and be significantly activated due to adsorption and subsequent hydrogenation reactions. In the next section we will explore various mechanistic pathways for ammonia and hydrazine synthesis that involve the aforementioned intermediates in order to explore low energy pathways that may occur at nitrogen vacancies of η - Mn_3N_2 .

View Article Online
DOI: 10.1039/C9CP03934A

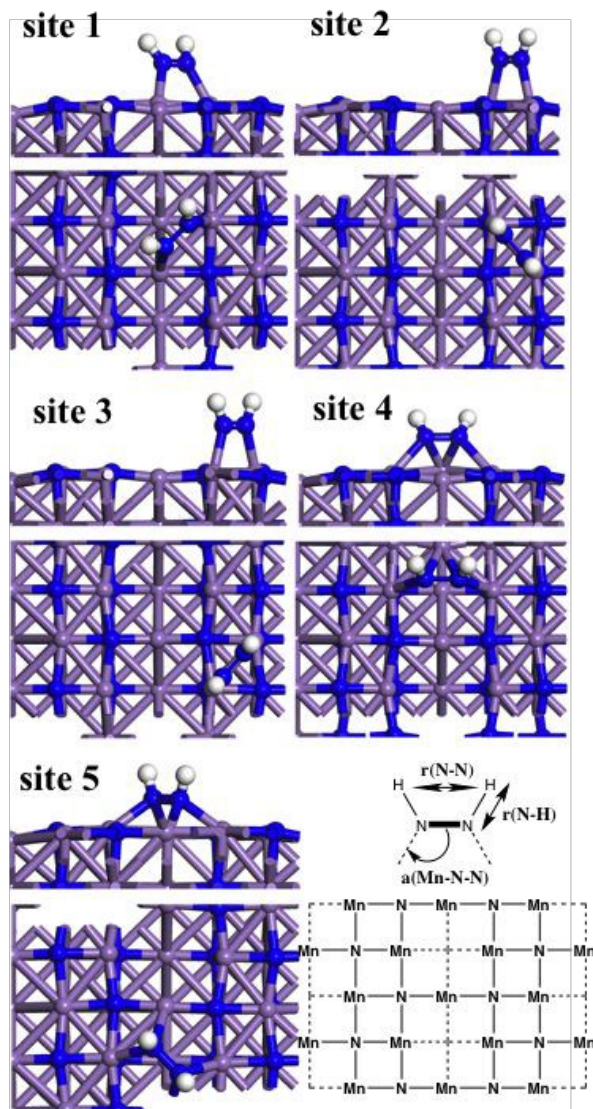


Figure 3. Side and top structures of HN=NH adsorbate on η -Mn₃N₂ surface. The N=NH adsorbate was bound to the same sites on this surface and the adsorption structures and energies are given in Table 3.

2.6 Reaction pathways for ammonia synthesis on η -Mn₃N₂-(100) surfaces

Based on the reaction intermediates identified in the previous sections we have modelled various potential mechanisms for ammonia and hydrazine synthesis on the (100) surface of η -Mn₃N₂. These reaction mechanisms are given in Fig. 4 to Fig. 7 and described in Scheme 2 to Scheme 5. In the first pathway (i.e. **Mechanism-1**) which synthesizes hydrazine via Langmuir-Hinshelwood chemistry and subsequently ammonia via Eley-Rideal chemistry, we find that the ammonia synthesis step is

prohibitive as its barrier (i.e. I to J in Fig. 4) is 153 kJ mol^{-1} which is relatively high to be overcome at moderate temperatures. Surprisingly though the mechanism for hydrazine synthesis on this catalysts appears facile as all the barriers for the reaction are in the range of 38 kJ mol^{-1} (i.e. A to C in Fig. 4) to 64 kJ mol^{-1} (i.e. D to E in Fig. 4) which are considerably lower than the Eley-Rideal mechanism step for ammonia synthesis seen in Scheme 2 step I to J. It is intriguing that this mechanism occurs entirely at a nitrogen vacancy on the (100) surface of $\eta\text{-Mn}_3\text{N}_2$ and that the adsorbed intermediate N_2 and $\text{HN}=\text{NH}$ both have the *side on* configurations as this is depicted in site 5 of Figure 3. In particular **Mechanism-1** which is the kinetically fastest for hydrazine synthesis among the four mechanisms studied starts with the side-on adsorption of N_2 to an intrinsic nitrogen vacancy of the (100) surface of $\eta\text{-Mn}_3\text{N}_2$ (i.e. A to B in Fig. 2 and Scheme 2). Molecular hydrogen then dissociatively chemisorbs at nearby Mn sites (i.e. B to C in Fig. 2 and Scheme 2), which due to the presence of unpaired electrons bind atomic hydrogen better than molecular hydrogen. This is followed by the dissociative adsorption of a second H_2 at another nearby Mn site (i.e. C to D in Fig. 2 and Scheme 2). These atomic H species can from this position react very efficiently through low barrier process with side-on adsorbed N_2 (which is depicted in Scheme 1) and subsequently form $\text{HN}=\text{NH}$ and hydrazine that is bound to the intrinsic nitrogen vacancy of $\eta\text{-Mn}_3\text{N}_2$. In particular, an atomic H moves from the Mn site to bind to side on adsorbed N_2 forming $>\text{N}=\text{NH}<$ (i.e. D to E in Fig. 2 and Scheme 2). This is followed by a second H transfer reaction on the other nitrogen forming $>\text{NH}=\text{NH}<$ (i.e. E to F in Fig. 2 and Scheme 2). Subsequently further hydrogenation occurs forming first $>\text{NH}-\text{NH}_2<$ (i.e. F to G in Fig. 2 and Scheme 2) and then hydrazine (i.e. G to H in Fig. 2 and Scheme 2). The subsequent further hydrogenation of hydrazine to ammonia appears energetically unfavourable and therefore this reaction mechanism is expected to saturate the surface of the catalysts with hydrazine which under high hydrogen feedstream should desorb the product hydrazine after flash annealing of the catalyst at moderate temperatures. These findings are in agreement with the previous study of the Eley-Rideal mechanism for ammonia synthesis on another manganese nitride, $\text{Mn}_6\text{N}_{5+x}(x=1)\text{-}(111)$ surfaces⁵³ which showed that these hydrogenation steps on manganese nitrides have relatively large barriers in contrast with what we had found on $\text{Co}_3\text{Mo}_3\text{N}$ surfaces¹³, in which the Eley-Rideal mechanism happens at moderate temperatures.

View Article Online
DOI: 10.1039/C9CP03934A

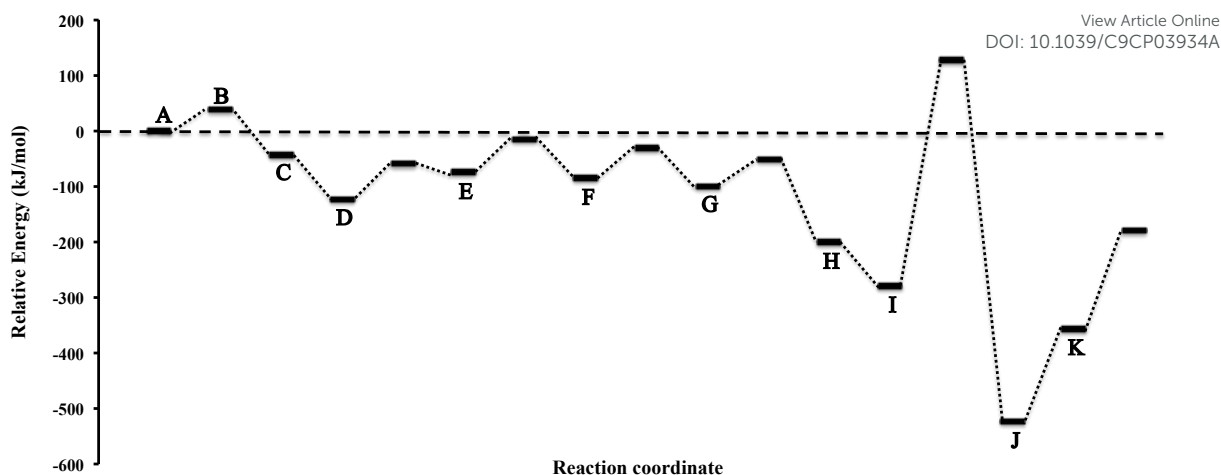
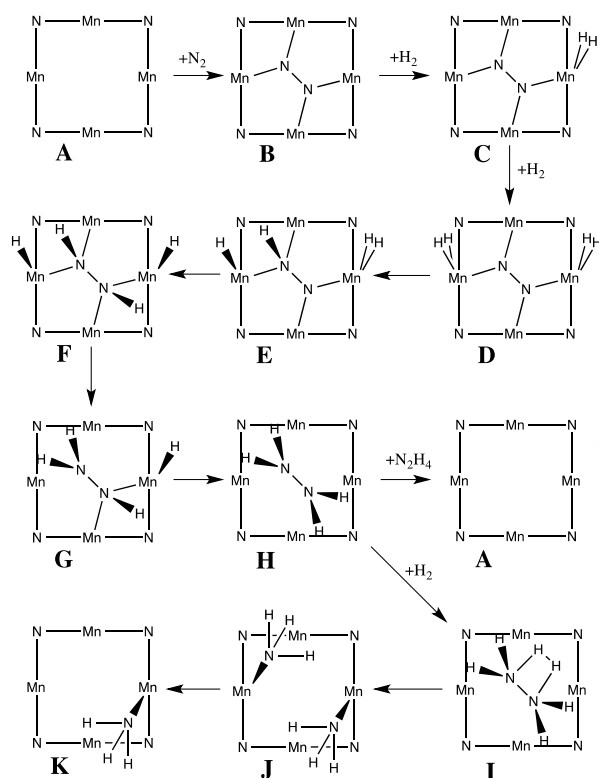


Fig. 4. **Mechanism-1** Potential energy diagram of hydrazine and ammonia synthesis reaction via a Langmuir–Hinshelwood and subsequent ammonia synthesis via an Eley–Rideal mechanism at intrinsic nitrogen vacancies on η - Mn_3N_2 .



Scheme 2. **Mechanism-1** Simplified schematic of the hydrazine synthesis reaction via a Langmuir–Hinshelwood mechanism and subsequent ammonia synthesis via an Eley–Rideal mechanism at intrinsic nitrogen vacancies on η - Mn_3N_2 .

In the second mechanism (**Mechanism-2**) N_2 that is adsorbed side on at the intrinsic nitrogen vacancies reacts directly with molecular hydrogen that originates from the gas phase. This is a typical Eley–Rideal mechanism for the hydrogenation of

N_2 which first forms $HN=NH$ (see M of Scheme 3) and subsequently hydrazine (see H of Scheme 3) which are both bound to the nitrogen vacancy side on. All three Eley-Rideal hydrogenation steps are very high, 298 kJ mol^{-1} , 491 kJ mol^{-1} and 409 kJ mol^{-1} , for the first, second and third hydrogenation steps, respectively. These barrier heights are in agreement with the barrier heights found on another manganese nitride, Mn_6N_{5+x} ($x = 1$)-(111) surfaces in a recent DFT-D3 study.⁵³ Due to the existence of such high hydrogenation barrier it is not expected that the ammonia or hydrazine synthesis would occur at moderate temperatures and therefore higher temperatures would become necessary. This clearly indicates that **Mechanism-1** would be the preferred route for the synthesis of ammonia and hydrazine as this can be seen by the comparison of the two potential energy curves.

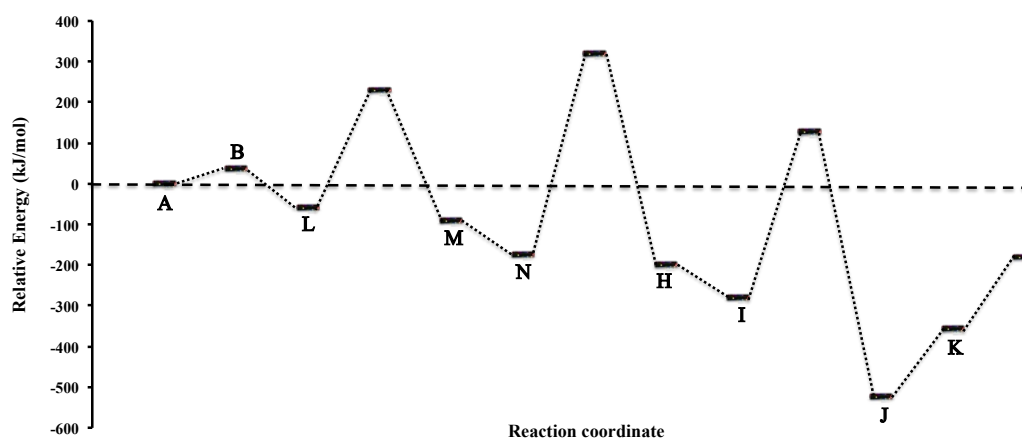
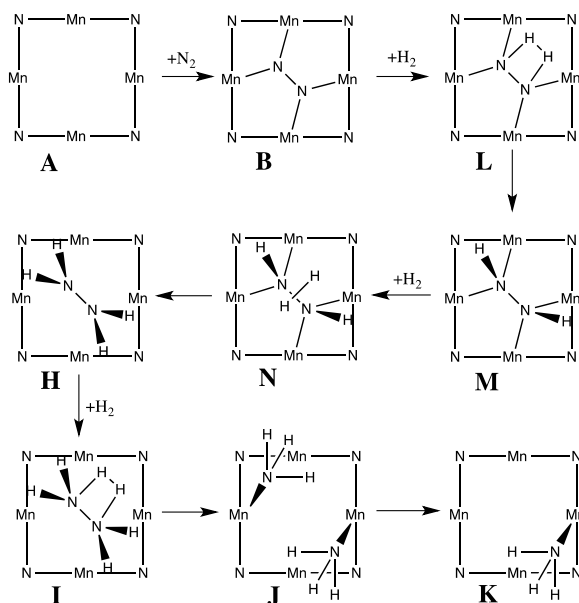


Fig. 5. **Mechanism-2** Potential energy diagram of the hydrazine and ammonia synthesis reaction via an Eley–Rideal mechanism at intrinsic nitrogen vacancies on η - Mn_3N_2 .



View Article Online
DOI: 10.1039/C9CP03934A

Scheme 3. **Mechanism-2** Simplified schematic of the hydrazine and ammonia synthesis reaction via an Eley-Rideal mechanism at intrinsic nitrogen vacancies on η - Mn_3N_2 .

In the third mechanism that we have computationally modelled (i.e. **Mechanism-3**) the first two hydrogenation steps occur via precursor-mediated state (notice adsorption energy of 99 kJ mol^{-1}) in which molecular H_2 is adsorbed molecularly *side-on* on one of the two nitrogens of N_2 (see O in Scheme 4) which later dissociates through a 316 kJ mol^{-1} barrier to form two N-H bonds on the same nitrogen atom. This forms an intermediate, which further hydrogenates by first adsorbing at a strength of 97 kJ mol^{-1} H_2 and subsequently dissociating it to form another two N-H bonds on two different nitrogen atoms, which forms an intermediate of the form $-\text{NHNH}_3$. This intermediate, similar to what was seen to occur at $\text{Co}_3\text{Mo}_3\text{N}$ nitrogen vacancies, release ammonia in an exothermic reaction step (see R to S in Scheme 4) forming an adsorbed N-H species at the intrinsic nitrogen vacancy site. Molecular H_2 then adsorbs at a nearby Mn site (see T in Scheme 4) with an adsorption energy of 101 kJ mol^{-1} . Here we notice that the barrier of the hydrogenation of $>\text{NH}_2$ from a nearby atomic H is rather small compared to the previous hydrogenation barriers. This barrier of hydrogenation is only 69 kJ mol^{-1} which clearly suggests that intrinsic nitrogen vacancies that are filled with nitrogen coming from the gas feed-stream will become vacant again through hydrogenation steps that involve atomically adsorbed H at nearby manganese sites, while producing ammonia. Such a mechanism of removal of surface nitrogen does not decompose the

metal nitride as this was suggested to be the case on Ta_3N_5 .⁵⁴ Furthermore it should maintain the concentration of surface nitrogen vacancies sufficiently high for the reaction to proceed at sufficiently high rates. Once ammonia is formed on the surface it is rather strongly bound with adsorption energy of 176 kJ mol^{-1} . The final state of this mechanism refers to the vacant initial active site $A + 2NH_3(g)$ (This applies to all four mechanisms studied).

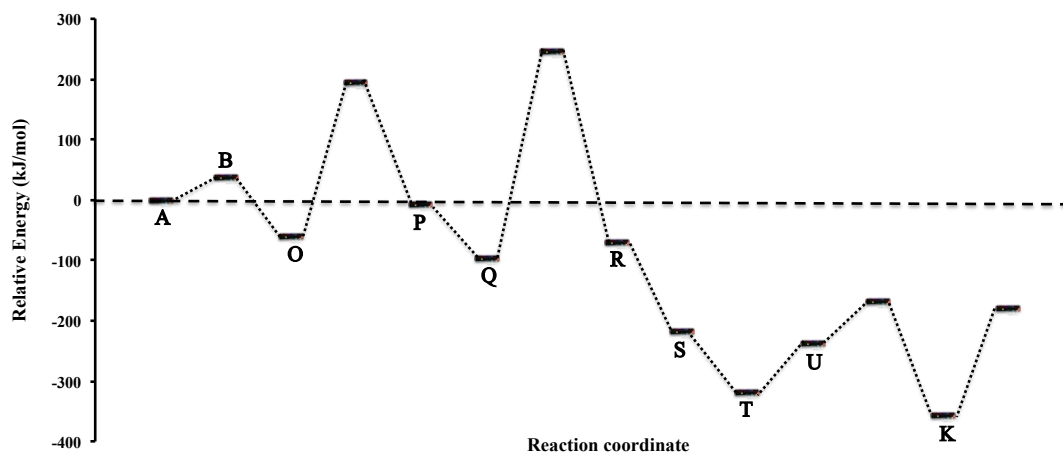
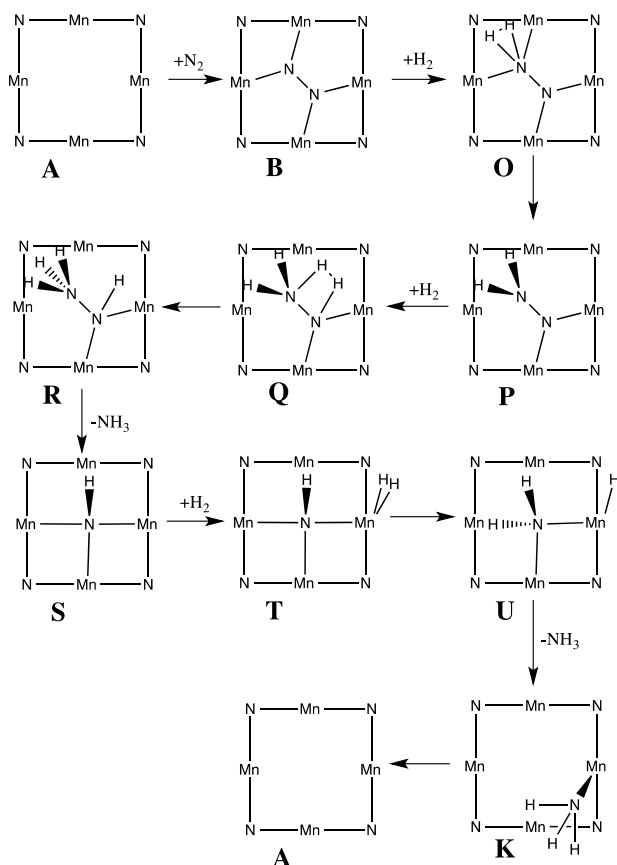


Fig. 6. **Mechanism-3** Potential energy diagram of the hydrazine and ammonia synthesis reaction via a precursor-mediated mechanism at intrinsic nitrogen vacancies on $\eta\text{-Mn}_3\text{N}_2$.



View Article Online
DOI: 10.1039/C9CP03934A

Scheme 4. **Mechanism-3** Simplified schematic of the hydrazine and ammonia synthesis reaction via a precursor-mediated mechanism at intrinsic nitrogen vacancies on η - Mn_3N_2 .

The fourth mechanism (i.e. **Mechanism-4**) shown in Fig. 7 for ammonia and hydrazine synthesis is rather similar to **Mechanism-3** shown in Fig. 6. It starts with the hydrogenation of surface activated N_2 via a precursor-mediated adsorption state (see O in Scheme 5) of molecular hydrogen. The hydrogenation barrier is comparatively high, 255 kJ mol^{-1} which suggest that the reaction pathway at moderate temperatures will be primarily **Mechanism-1** that has low barriers until the formation of hydrazine and that **Mechanism-2**, **Mechanism-3** and **Mechanism-4**, will be minor side reactions of the equilibrium that will establish on the catalyst when steady-state conditions are reached. As seen in **Mechanism-3** the dissociative adsorption of the second hydrogen molecule is exothermic (see P to V in Scheme 5 and Figure 7) by 89 kJ mol^{-1} and it forms Mn-H species that can further hydrogenate the N-N bond. This hydrogenation step has a moderate barrier which is 85 kJ mol^{-1} which forms an intermediate of the form $-\text{NHNH}_2$. At this point in the mechanism a H-transfer reaction results in the formation of $-\text{NNH}_3$, which readily decomposes forming

ammonia and filling up the nitrogen vacancy site with four-fold bond nitrogen (see Y in Scheme 5). It is noted that this H-transfer reaction (G to X in Scheme 5) has a rather large barrier (i.e. 210 kJ mol⁻¹). Therefore **Mechanism-4** has the opposing tendency of **Mechanism-3** to fill the nitrogen vacancies whereas the latter will constantly form such vacancies. Due to the similar barrier heights in **Mechanism-3** and **Mechanism-4** these two reactions will be in a dynamic equilibrium keeping the concentration of *intrinsic* and *extrinsic* nitrogen-vacancies constant. In contrast to the high barrier for H-transfer found for >NHNH₂ to form >NNH₃ the hydrogen transfer to form four-fold bound -NH from four-fold bound -N is only 75 kJ mol⁻¹. Subsequent dissociative adsorption of H₂ at a nearby manganese site is exothermic (see T in Fig. 7) by 134 kJ mol⁻¹. Then the barrier for H-transfer to -NH in order to form -NH₂ is a high barrier process (187 kJ mol⁻¹) and therefore would occur only at high temperatures. Further hydrogenation of -NH₂ via hydrogen transfer from Mn-H has a much smaller barrier (69 kJ mol⁻¹) than the previous hydrogenation step. This results in the formation of surface bound ammonia which has a large endothermic desorption energy of 176 kJ mol⁻¹.

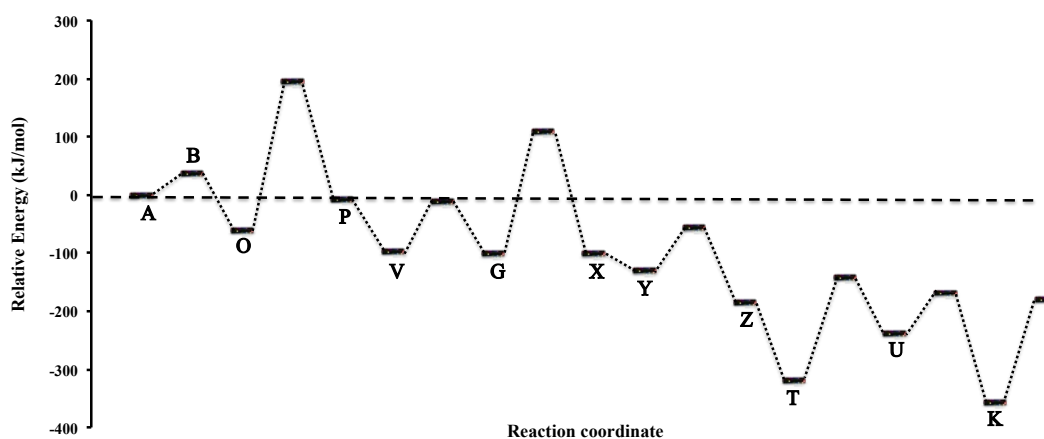
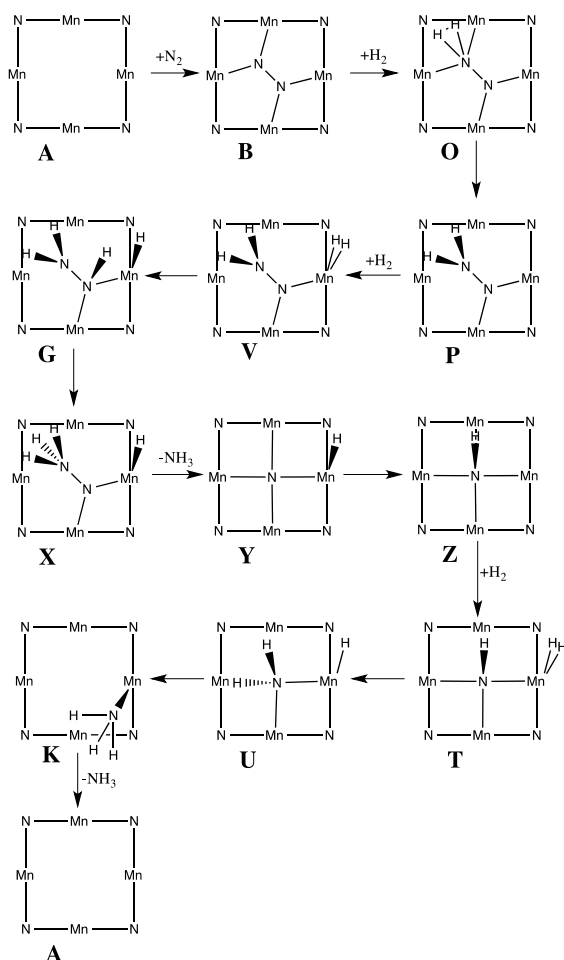


Fig. 7. **Mechanism-4** Potential energy diagram of the hydrazine and ammonia synthesis reaction via a precursor-mediated mechanism at intrinsic nitrogen vacancies on η -Mn₃N₂.



View Article Online
DOI: 10.1039/C9CP03934A

Scheme 5. **Mechanism-4** Simplified schematic of the hydrazine and ammonia synthesis reaction via a precursor-mediated mechanism at intrinsic nitrogen vacancies on η - Mn_3N_2 .

Conclusions

This work is a comprehensive study of the various mechanistic pathways for ammonia and hydrazine synthesis on η - Mn_3N_2 . We have used dispersion-corrected hybrid DFT calculations to calculate potential Eley-Rideal and Langmuir-Hinshelwood mechanisms for ammonia and hydrazine synthesis on η - Mn_3N_2 -(100) surfaces. The revPBE-D3 calculations clearly point to a low barrier Langmuir-Hinshelwood mechanism for hydrazine synthesis, which occurs at intrinsic nitrogen vacancies on the (100) surface. Additional Eley-Rideal mechanisms for ammonia synthesis appear to have high barriers for the hydrogenation steps and are therefore not possible at moderate temperatures. The simulations of the various intermediates was assisted by Lewis structure algorithm and cluster calculations which helped to offer the spectroscopic IR signatures of the various intermediates using hybrid DFT with a relatively large basis set. Furthermore, the calculated IR oscillator frequencies

and intensities may assist in the experimental identification of the adsorbates on actual manganese nitride catalysts using surface IR spectroscopies.

View Article Online
DOI: 10.1039/C9CP03934A

AUTHOR INFORMATION

Corresponding Author

*c.zeinalipouryazdi@greenwich.ac.uk

Supporting Information

The Cartesian coordinates of the structure of the various cluster-adsorbates (Figure S1) and the fractional coordinates of the various surface-adsorbate slabs (Figure S2) are given as supporting information.

ACKNOWLEDGMENTS

This study was supported by EPSRC funding (EP/L026317/1, EP/K014714/1). Via our membership of the UK's HEC Materials Chemistry Consortium, which is funded by EPSRC (EP/L000202/1), this work used the ARCHER UK National Supercomputing Service (<http://www.archer.ac.uk>). The authors acknowledge the use of the Grace High Performance Computing Facility (Grace@UCL), and associated support services, in the completion of this work.

REFERENCES

- (1) Haber, F. *Naturwissenschaften* **1922**, *10*, 1041.
- (2) Haber, F. *Naturwissenschaften* **1923**, *11*, 339.
- (3) Smil, V. *Enriching the Earth: Fritz Haber, Carl Bosch, and the Transformation of World Food Production*; MIT Press: Cambridge, MA, 2004.
- (4) Pfromm, P. H. J. *Renew. Sust. Energ.* **2017**, *9*, 034702.
- (5) Saadatjou, N.; Jafari, A.; Sahebdehfar, S. Ruthenium Nanocatalysts for Ammonia Synthesis: A Review. *Chemical Engineering Communications* **2015**, *202*, 420-448.
- (6) Zeinalipour-Yazdi, C. D.; Hargreaves, J. S.; Laassiri, S.; Catlow, C. R. A. The integration of experiment and computational modelling in heterogeneously catalysed ammonia synthesis over metal nitrides. *Phys. Chem. Chem. Phys.* **2018**, *20*, 21803-21808.
- (7) Boisen, A.; Dahl, S.; Jacobsen, C. J. H. Promotion of Binary Nitride Catalysts: Isothermal N₂ Adsorption, Microkinetic Model, and Catalytic Ammonia Synthesis Activity. *J. Catal.* **2002**, *208*, 180-186.
- (8) Jacobsen, C. J. H. Novel Class of Ammonia Synthesis Catalysts. *Chem. Commun.* **2000**, 1057-1058.

- (9) Jacobsen, C. J. H.; Dahl, S.; Clausen, B. S.; Bahn, S.; Logadóttir, A.; J. Nørskov, View Article Online
DOI: 10.1039/C9CP03934A
Catalyst Design by Interpolation in the Periodic Table: Bimetallic Ammonia Synthesis Catalysts. *J. Am. Chem. Soc.* **2001**, *123*, 8404-8405.
- (10) Kojima, R.; Aika, K.-I. Cobalt Molybdenum Bimetallic Nitride Catalysts for Ammonia Synthesis. *Chem. Lett.* **2000**, 514-515.
- (11) Kojima, R.; Aika, K.-I. Cobalt Molybdenum Bimetallic Nitride Catalysts for Ammonia Synthesis: Part 1. Preparation and Characterization. *Appl. Catal. A: Gen.* **2001**, *215*, 149-160.
- (12) Jacobsen, C. J. H.; Dahl, S.; Clausen, B. S.; Bahn, S.; Logadóttir, A.; Nørskov, J. *J. Am. Chem. Soc.* **2001**, *123*, 8404-8405.
- (13) Zeinalipour-Yazdi, C. D.; Hargreaves, J. S. J.; Catlow, C. R. A. Low-T Mechanisms of Ammonia Synthesis on Co₃Mo₃N. *J. Phys. Chem. C* **2018**, *122*, 6078-6082.
- (14) Zeinalipour-Yazdi, C. D.; Hargreaves, J. S. J.; Catlow, C. R. A. DFT-D3 Study of Molecular N₂ and H₂ Activation on Co₃Mo₃N Surfaces. *J. Phys. Chem. C* **2016**, *120*, 21390-21398.
- (15) Abghoui, Y.; Garden, A. L.; Hlynsson, V. F.; Bjorgvinsdottir, S.; Olafsdottir, H.; Skulason, E. Enabling Electrochemical Reduction of Nitrogen to Ammonia at Ambient Conditions Through Rational Catalyst Design. *Phys. Chem. Chem. Phys.* **2015**, *17*, 4909-4918.
- (16) Abghoui, Y.; Garden, A. L.; Howat, J. G.; Vegge, T.; Skulason, E. Electroreduction of N₂ to Ammonia at Ambient Conditions on Mononitrides of Zr, Nb, Cr, and V: A DFT Guide for Experiments. *ACS Catal.* **2016**, *6*, 635-646.
- (17) Michalsky, R.; Pfromm, P. H.; Steinfeld, A. Rational Design of Metal Nitride Redox Materials for Solar-Driven Ammonia Synthesis. *Interface Focus* **2015**, *5*, 20140084-10.
- (18) Michalsky, R.; Avram, A. M.; Peterson, B. A.; Pfromm, P. H.; Peterson, A. A. Chemical Looping of Metal Nitride Catalysts: Low-Pressure Ammonia Synthesis for Energy Storage. *Chem. Sci.* **2015**, *6*, 3965-3974.
- (19) Ertl, G. Surface Science and Catalysis—Studies on the Mechanism of Ammonia Synthesis: The P. H. Emmett Award Address. *Surf. Sci. Catal.* **1980**, *21*, 201-223.
- (20) Bowker, M. Modelling of ammonia synthesis kinetics. *Catal. Today* **1992**, *12*, 153-163.
- (21) Logadóttir, Á.; Nørskov, J. K. *J. Catal.* **2003**, *220*, 273-279.
- (22) Zhang, C. J.; Lynch, M.; Hu, P. *Surf. Sci.* **2002**, *496*, 221-230.
- (23) Garden, A. L.; Skúlason, E. *J. Phys. Chem. C* **2015**, *119*, 26554-26559.
- (24) Abghoui, Y.; Skúlason, E. Electrochemical synthesis of ammonia via Mars-van Krevelen mechanism on the (111) facets of group III-VII transition metal mononitrides. *Catal. Today* **2017**, *286* 78-84.
- (25) Leineweber, A.; Niewa, R.; Jacobs, H.; Kockelmann, W. The Manganese Nitrides Eta-Mn₃N₂ and Theta-Mn₆N_{5+x}: Nuclear and Magnetic Structures. *J. Mater. Chem.* **2000**, *10*, 2827-2834.
- (26) Laassiri, S.; Zeinalipour-Yazdi, C. D.; Catlow, C. R. A.; Hargreaves, J. S. J. The potential of manganese nitride based materials as nitrogen transfer reagents for nitrogen chemical looping. *Applied Catalysis B: Environmental* **2018**, *223*, 60-66.
- (27) Monkhorst, H. J.; Pack, J. D. Special Points for Brillouin-Zone Integrations. *Phys. Rev. B* **1976**, *13*, 5188-5192.

- (28) Kresse, G.; Furthmüller, J. Efficient Iterative Schemes for *ab initio* Total Energy Calculations Using a Plane-Wave Basis Set. *Phys. Rev. B* **1996**, *54*, 11169–11186. View Article Online
DOI: 10.1039/C9CP03934A
- (29) Kresse, G.; Hafner, J. *Ab initio* Molecular Dynamics for Liquid Metals. *Phys. Rev. B* **1993**, *47*, 558-561.
- (30) Perdew, J. P.; Burke, K.; Ernzerhof, M. Generalized Gradient Approximation Made Simple. *Phys. Rev. Lett.* **1996**, *77*, 3865-3868.
- (31) Kresse, G.; Joubert, D. From Ultrasoft Pseudopotentials to the Projector Augmented-Wave Method. *Phys. Rev. B* **1999**, *59*, 1758–1775.
- (32) Blöchl, P. E. Projector Augmented-Wave Method. *Phys. Rev. B* **1994**, *50*, 17953-17979.
- (33) Grimme, S.; Antony, J.; Ehrlich, S.; Krieg, H. A Consistent and Accurate *ab initio* Parametrization of Density Functional Dispersion Correction (DFT-D) for the 94 Elements H-Pu. *J. Chem. Phys.* **2010**, *132*, 154104.
- (34) Mills, G.; Jónsson, H.; Schenter, G. K. Reversible Work Transition State Theory: Application to Dissociative Adsorption of Hydrogen. *Surf. Sci.* **1995**, *324*, 305-337.
- (35) Leineweber, A.; Niewa, R.; Jacobs, H.; Kockelmann, W. The manganese nitrides η -MnN and θ -MnN: nuclear and magnetic structures. *J. Mater. Chem.* **2000**, *10*, 2827-2834.
- (36) Laassiri, S.; Zeinalipour-Yazdi, C. D.; Catlow, C. R. A.; Hargreaves, J. S. J. The potential of manganese nitride based materials as nitrogen transfer reagents for nitrogen chemical looping. *Appl. Catal. B: Environ.* **2018**, *223*, 60-66.
- (37) Gaussian 09, R. C., M. J. Frisch, G. W. Trucks, H. B. Schlegel, G. E.; Scuseria, M. A. R., J. R. Cheeseman, G. Scalmani, V. Barone, B. Mennucci, G. A. Petersson, M. C. Gaussian Inc.: Wallingford CT, 2009.
- (38) Becke, A. D. Density-Functional Thermochemistry. III. The Role of Exact Exchange. *J. Chem. Phys.* **1993**, *98*, 5648.
- (39) Lee, C.; Yang, W.; Parr, R. G. Development of the Colle-Salvetti Correlation-Energy Formula Into a Functional of the Electron Density. *Phys. Rev. B* **1988**, *37*, 785-789.
- (40) Woon, D. E.; Dunning Jr., T. H. Gaussian Basis Sets for Use in Correlated Molecular Calculations. III. The Atoms Aluminum Through Argon. *J. Chem. Phys.* **1993**, *98*, 1358.
- (41) Wilson, A.; van Mourik, T.; Dunning Jr., T. H. Gaussian Basis Sets for Use in Correlated Molecular Calculations. VI. Sextuple Zeta Correlation Consistent Basis Sets for Boron Through Neon. *J. Mol. Struct.* **1997**, *388*, 339-349.
- (42) Peterson, K. A.; Woon, D. E.; Dunning Jr., T. H. Benchmark Calculations With Correlated Molecular Wave Functions. IV. The Classical Barrier Height of the $H+H_2 \rightarrow H_2+H$ Reaction. *J. Chem. Phys.* **1994**, *100*, 7410.
- (43) Kendall, R. A.; Jr., T. H. D.; Harrison, R. J. Electron Affinities of the First - Row Atoms Revisited. Systematic Basis Sets and Wave Functions. *J. Chem. Phys.* **1992**, *96*, 6796.
- (44) Dunning Jr., T. H. Gaussian Basis Sets for Use in Correlated Molecular Calculations. I. The Atoms Boron Through Neon and Hydrogen. *J. Chem. Phys.* **1989**, *90*, 1007.
- (45) Stevens, W.; Basch, H.; Krauss, J. Compact effective potentials and efficient shared - exponent basis sets for the first - and second - row atoms. *J. Chem. Phys.* **1984**, *81*, 6026.

- (46) Cundari, T. R.; Stevens, W. J. Effective core potential methods for the lanthanides. *J. Chem. Phys.* **1993**, *98*, 5555. View Article Online
DOI:10.1039/C9CP03934A
- (47) Stevens, W. J.; Krauss, M.; Bausch, H.; P. G. Jasien Relativistic compact effective potentials and efficient, shared-exponent basis sets for the third-, fourth-, and fifth-row atoms. *Can. J. Chem.* **1992**, *70*, 612-630.
- (48) Lewis, G. N. The Atom and the Molecule. *J. Am. Chem. Soc.* **1916**, *38*, 762-785.
- (49) Zeinalipour-Yazdi, C. D.; Hargreaves, J. S. J.; Laassiri, S.; Catlow, C. R. A. DFT-D3 Study of H₂ and N₂ Chemisorption Over Cobalt Promoted Ta₃N₅-(100), (010) and (001) Surfaces. *Phys. Chem. Chem. Phys.* **2017**, *19*, 11968-11974.
- (50) Cioslowski, J. A New Population Analysis Based on Atomic Polar Tensors. *J. Am. Chem. Soc.* **1989**, *111*, 8333-8336.
- (51) Silverstein, R. M.; Bassler, G. C.; Morrill, T. C. *Spectrometric Identification of Organic Compounds*, 4th ed ed.; John Wiley and Sons: New York, 1981.
- (52) Blanksby, S. J.; Ellison, G. B. Bond Dissociation Energies of Organic Molecules. *Acc. Chem. Res.* **2003**, *36*, 255-263.
- (53) Zeinalipour-Yazdi, C. D. On the possibility of an Eley-Rideal mechanism for ammonia synthesis on Mn₆N_{5+x} (x = 1)-(111) surfaces. *Phys. Chem. Chem. Phys.* **2018**, *20*, 18729-18736.
- (54) Zeinalipour-Yazdi, C. D.; Hargreaves, J. S. J.; Laassiri, S.; Catlow, C. R. A. DFT-D3 study of H₂ and N₂ chemisorption over cobalt promoted Ta₃N₅-(100), (010) and (001) surfaces. *Phys. Chem. Chem. Phys.* **2017**, *19*, 11968-11974.

The mechanisms of ammonia and hydrazine synthesis have been studied on (100) surfaces of Mn_3N_2 View Article Online
DOI:10.1039/C9CP03934A

